Exploiting Multi-Direction Features in MRF-Based Image Inpainting Approaches

ZHIDAN LI[ID], JIAWEI LIU[ID], AND JIXIANG CHENG[ID]

School of Electrical Engineering and Information, Southwest Petroleum University, Chengdu 610500, China

Corresponding author: Zhidan Li (dan.807@163.com)

ABSTRACT Image inpainting technique recovers the missing regions of an image using information from known regions and it has shown success in various application fields. As a popular kind of methods, Markov Random Field (MRF)-based methods are able to produce better results than earlier diffusion-based and sparse-based methods on inpainting images with big holes. However, for images with complex structures, the results are still not quite pleasant and some inpainting trails exist. The direction feature is an important factor for image understanding and human eye visual requirements, and exploiting multi-direction features is of great potential to further improve inpainting performance. Following the idea, this paper proposes a Structure Offsets Statistics based image inpainting algorithm by exploiting multiple direction features under the framework of MRF-based methods. Specifically, when selecting proper labels, multi-direction features are extracted and applied to construct a structure image and a non-structure image, and the candidate labels are chosen from the offsets of structure and non-structure images. Meanwhile, the multi-direction features are applied to construct a new smooth term for the energy equation which is then solved by graph-cut optimization technology. Experimental results show that on inpainting tasks with various complexities, the proposed method is superior to several state-of-the-art approaches in terms of the abilities of maintaining structure coherence and neighborhood consistence and the computational efficiency.

INDEX TERMS Image inpainting, multi-direction feature, Markov random field, structure offsets statistics.

I. INTRODUCTION

Image inpainting, also known as image completion, image restoration and image disocclusion, aims to recover the missing or degraded regions of an image in a visually plausibly way by using the known pixels of the image [1]. Nowadays, image inpainting is an active research topic in computer vision and image processing and has been applied in areas ranging from image editing, image transmission to film postproduction and ancient painting protection [2]. Although image inpainting technique is very useful, it is far from being solved perfectly and more effective approaches are deserved to be investigated.

A mount of methods with unique features have been devised by mathematicians or computer scientists, which can be classified into diffusion-based, sparse-based, exemplar-based and deep learning-based methods.

The diffusion-based methods, focusing on filling narrow or small holes, diffuse known information into missing regions based on partial differential equation theory, such as BSCB model [1], Navier-stokes model [3], total variation model [4], and curvature-driven diffusions [5]. This kind of methods perform poorly on inpainting images with structure or texture missing regions. The sparse-based methods reconstruct an image based on sparse representation theory, and serval techniques were applied such as super-wavelet transform [6], [7], dictionary library construction [8], [9], and low-rank matrix completion [10]–[12]. Although performing better than diffusion-based methods, sparse-based methods fail to recover structure and texture when dealing with large missing regions. To tackling the deficiency, the exemplar-based methods were proposed, which propagate information from source regions into missing regions at patch level. According to implementation way, the methods can be grouped into two categories, i.e., greedy-based and Markov Random Field (MRF)-based methods. The greedy-based methods include

The associate editor coordinating the review of this manuscript and approving it for publication was You Yang[ID].

two procedures, i.e., priority function design for filling order determination and match criteria design, and serval works were devoted on the procedures [13]–[18]. The defects of greedy-based methods are inevitable error propagation phenomenon and high computational overhead. The MRF-based methods alleviate error accumulation phenomenon by formulating image inpainting as a discrete MRF optimization problem [19], [20], and have shown an advantage over other kinds of methods. In addition, with the rise of deep learning technique, some researchers applied deep learning for image inpainting task and got competitive inpainting results [21]–[25]. However, deep learning requires huge computation power and a large number of sample images, which may limits its wide applications.

Nowadays, MRF-based methods are the mainstream algorithms for image inpainting tasks. In the methods, a known pixel/patch and a missing pixel/patch are respectively regarded as a label and a node, and the inpainting problem becomes assigning a suitable label to a node under certain criteria. Usually, the labels can be thought as absolute locations or relative offsets. In [20], all relative offsets are considered as labels to repair missing regions. However, the method introduces inappropriate labels and produces unpleasant inpainted results, and it is computationally intensive. To effectively and efficiently generate labels, He and Sun [26] proposed to select a few dominant offsets according to the statistics of patch offsets. Xue and Zhang [27] applied HOG features to calculate offsets statistics. Liu and Caselles [28] adopted neighboring offsets as candidate labels according to the local self-similarity. Ružić and Pižurica [29] selected labels from the most contextually similar blocks. Ge *et al.* [30] designed a sparse patch subspace learning method to select candidate labels. In addition to labels selection, energy equation affects the final results heavily and some researchers reformulate energy equation in order to obtain better results. For example, Gupta *et al.* [31] incorporated long range pairwise potentials into energy equation in order to capture the inherent repeating patterns for inpainting heritage architectural images. Bugeau *et al.* [32] considered three factors in energy equation, including self-similarity, diffusion and coherence of images. Liu and Caselles [28] adopted gradient information in the energy function to compensate high frequency information loss. Ghorai *et al.* [33] applied the dissimilarity between candidate patch and corresponding refined patch to construct energy equation.

Commonly, human eye is sensitive to the loss of high frequency information, such as edge, corner and structure, and neighborhood consistence reflects the naturalness of inpainted images. Therefore, structure coherence and neighborhood consistence should be highly regarded. Regarding to MRF-based methods, though many works [26]–[29], [33], [34] addressed the issues to some extent from various perspectives, there are still much room for further improving inpainting performance. Particularly, when degraded images have only a few known structures, these methods could not work effectively. Thus, how to achieve sufficient priori

information from limited known information to guide inpainting process is crucial for obtained pleasant results. Image features, related to different properties of an image, provide rich information on image content, and they are fundamental in many image analysis tasks like recognition and matching. Therefore, extracting more suitable image features to guide the inpainting process is a feasible way to enhance the inpainting performance especially for images with large missing regions, and such a routing has been explored in literatures and yielded some benefits. For example, Xue and Zhang [27] applied HOG features for matching similar patches. Liu and Caselles [28] utilized gradient feature to select a label for a node. Jin and Bai [35] introduced first-order directional derivative of facet model to find candidate patches. In our work [16], we designed a weighted color-direction feature to find the most similar patches for sparse representation. In our previous work [36], we devised a direction structure distribution analysis scheme to select candidate labels, and it works well for images with linear structures. However, for degraded images with complex structures, the method could not yield pleasant results.

With the purposes of better maintaining structure coherence and neighborhood consistence for completing degraded images with large missing regions, this paper proposes a Structure Offsets Statistics based inpainting algorithm (Abbreviated as SOS) via in-depthly exploiting image direction features to guide inpainting process under the framework of MRF-based methods. The main contributions of this paper are as follows.

(1) To better maintain structure coherence, the image is partitioned into structure and non-structure parts according to multi-direction features obtained by Curvelet transform, and the offsets are counted independently in these two parts. Then, a few dominant ones are chosen as candidate labels.

(2) To better maintain neighborhood consistence, instead of only using color information, multi-direction features based on Curvelet transform are exploited to construct energy equation.

(3) Experimental results demonstrate the superiority of our method over serval state-of-the-art methods on five kinds of inpainting tasks, and the effectiveness of proposed two schemes are empirically validated.

The rest of this paper is organized as follows. Section II presents the framework of MRF-based methods. Section III details the proposed algorithm, including labels selection, energy equation construction, and a brief analysis of the method. Section IV presents the experimental results on a variety of images as well as an empirical analysis. Finally, conclusions are made in Section V.

II. FRAMEWORK OF MRF-BASED METHODS
Given a degraded image I with missing region Ω, a pixel/patch p located at position $x = (x, y)$ in missing region is filled with a certain pixel/patch q located at position $x + o$ from known region, where $o = (u, v)$ is an offset. Therefore, the inpainting problem is how to assign
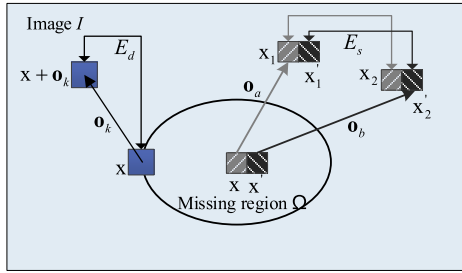
FIGURE 1. Sketch of energy function.

a suitable offset o to each unknown pixel/patch at x. Given the offsets, the inpainted image can be obtained by combining a stack of shifted images corresponding to these offsets. In MRF-based methods, the known pixels/patches and the missing pixels/patches are regarded as labels and nodes, and how to assign labels or offsets is implemented by minimizing the energy equation

$$E(L) = \sum_{x \in \Omega} E_d(L(x)) + \sum_{x,x' \in \Omega} E_s(L(x), L(x')) \quad (1)$$

where the neighboring pixels/patches (x, x') are 4-connected; the argument $L(\cdot)$ is a labeling map which assigns a label from a pre-selected offsets set $\{o_i\}$ to the unknown pixel/patch at position x, e.g., $L(x) = i$ means the missing pixel/patch at x is filled with the pixel/patch at $x + o_i$. A sketch of energy equation is illustrated in Figure 1. The data term E_d, which aims to maintain structure coherence, is 0 if label o_i is valid for x, i.e., $x + o_i$ locating at the known region; otherwise E_d is $+\infty$. The smooth term E_s aims to maintain neighborhood consistence. In the original work [20], the smooth term E_s is defined as

$$E_s(a, b) = \|I(x + o_a) - I(x + o_b)\|^2 + \|I(x' + o_a) - I(x' + o_b)\|^2 \quad (2)$$

where $I(x)$ is the RGB color value of x; $I(\cdot + o_i)$ is an image shifted by o_i. If $o_a \neq o_b$, the neighboring pixels/patches x and x' will be assigned different labels, resulting a seam between x and x'. Hence, equation (2) penalizes neighboring labels if two shifted images $I(x + o_a)$ and $I(x + o_b)$ are not similar near this seam. Then energy equation (1) is optimized using multi-label graph-cuts technique [37]. For more information of MRF-based methods, refer to [26].

When solving energy equation (1), utilizing all known offsets as candidate offsets may not produce pleasant results. On the one hand, some unsuitable offsets may bring in interference during optimization process, resulting in unsatisfactory inpainting performance like structure incoherence. On the other hand, only the color information is considered in smooth term, which may lead to neighborhood inconsistence. To tackling the two issues, selecting a few but more reasonable offsets from all known offsets as candidates is a robust way to enhance inpainting performance and computational efficiency. Meanwhile, integrating more information in energy equation is able to better satisfy

human eye visual requirements. Based on the considerations, we proposed a new MRF-based method through in-depthly exploiting multi-direction features, which is expounded in the next section.

III. THE PROPOSED ALGORITHM

To better maintain structure coherence and neighborhood consistence of the inpainted results, this paper proposes a structure offsets statistics based image inpainting algorithm using multi-direction features. The two main procedures as well as an analysis of the method are detailed in this section.

A. LABELS SELECTION

The procedure of our labels selection is sketched in Figure 2. We first apply Curvelet forward transform on the image to obtain coefficient matrixes with different directions and scales, and the coefficient matrixes are partitioned into different direction sets. For each set, only the large coefficients are utilized to perform Curvelet reverse transform to reconstruct a direction image. Then the structure part of the degraded image is constructed by stacking the plentiful edge information of direction images, and the left part is treated as non-structure part. Afterwards, the offsets are independently counted for structure and non-structure parts, and a few dominant offsets are chosen as candidate labels. In what follows, we explain the procedure in detail. Let the input image denoted as I_Y, which is the Y component of original color image I in YUV space. Multi-direction and multi-scale Curvelet decomposition is performed on I_Y, that is,

$$Q = T^+(I_Y) \quad (3)$$

where T^+ implies Curvelet forward transform and $Q = \{Q_{s,d}\}$ is the coefficient matrix set with scale s and direction d. In this paper, the coefficient matrix scale s is set to 5, and the numbers of direction matrix for five scales are respectively set to 1, 16, 32, 32, and 64. An illustration of Curvelet coefficients partition is presented in Figure 3. The coefficient matrix $Q_{1,1}$ represents low frequency information of an image, and the others represent high frequency information of different degrees over different directions. In order to accurately capture high frequency information like structures and edges, for two to five scales, only the coefficients larger than a threshold are applied for further processing, formulated as

$$Q'_{s,d}(r, c) = \begin{cases} 0, & \text{if } Q_{s,d}(r, c) < \alpha \cdot \max\{|\Psi(r, c)|\} \\ Q_{s,d}(r, c), & \text{otherwise.} \end{cases} \quad (4)$$

where $\Psi(r, c)$ is a patch centered at (r, c) with a size of 11×11, and α is a coefficient regulating the threshold. The value of α impacts final inpainting performance and how to set a proper value will be discussed in Section IV-A.

Then Curvelet coefficient matrix set $Q' = \{Q'_{s,d}\}$ from the second to fifth scale layers (i.e., $s = 2, \cdots, 5$) is partitioned into N sets according to N directions. An illustration of the partition with 8 directions is given in Figure 3(b).
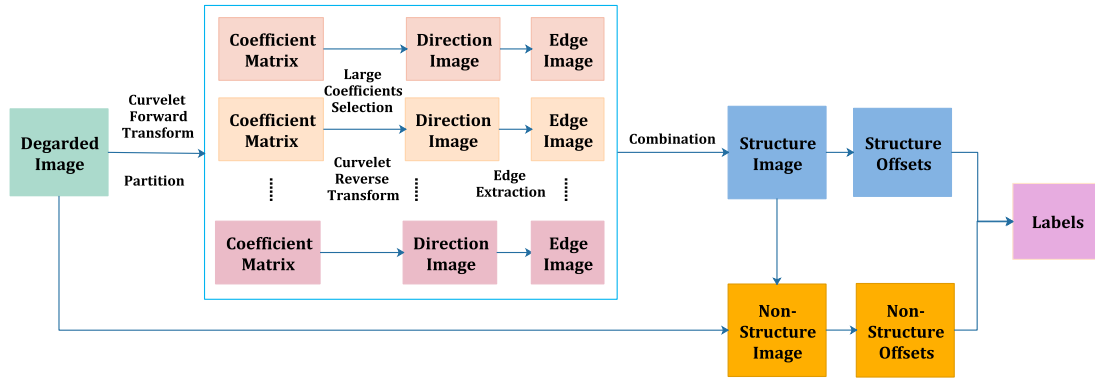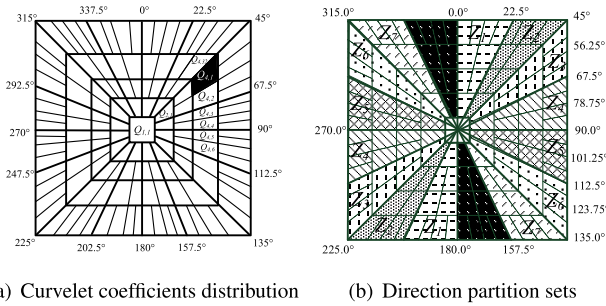
FIGURE 2. The frame diagram of label selection.

FIGURE 3. An illustration of curvelet coefficients partition.

(a) Curvelet coefficients distribution   (b) Direction partition sets

The set Z_1 does not only include the features exactly at 0° or horizontal direction of an image, but regions ranging from 0° to 22.5° and from 180° to 202.5°, and similar for other seven sets. On this basis, the direction image $A_n(n = 1, \cdots, N)$ over the n-th direction can be inferred via

$$A_n = T^-(Z_n \cup Q_{1,1}) \qquad (5)$$

where the size of A_n equals to the size of I_Y and T^- denotes Curvelet inverse transform. To extract plentiful edge information, canny operator and morphological operation are performed on each A_n, resulting edge images denoted as B_n. Then a whole edge image B is generated by stacking B_n, i.e., $B = \cup_{n=1}^N B_n$. Therefore, we can obtain plentiful structure information,which is beneficial for maintaining structure coherence. According to B, the image I is partitioned into structure part I_s via $I_s = I \cdot B$ and non-structure part I_{ns} via $I_{ns} = I \backslash I_s$.

Afterwards, we respectively match similar patches in I_s and I_{ns} to obtain the offsets. Specifically, for each patch $P(x)$ with a size of 8×8 in known region of I_s, we compute its offset $O_s(x)$ to its most similar patch measured by the sum of squared distance between two patches, that is,

$$O_s(x) = \underset{o}{\operatorname{argmin}} \|P(x + o) - P(x)\|, s.t. \|o\| > \tau \qquad (6)$$

where $o = (u, v)$ is a 2-d coordinates of an offset, $x = (x, y)$ is the center position of patch $P(x)$, τ is a threshold to preclude nearby patches and usually set to 8. To efficiently compute offsets, traditional KD-trees method is applied to find the nearest neighbor field additionally rejecting any

patch that disobeys the constraint during the search procedure. In addition, based on local similarity, the search region is adaptively decided according to the size of missing region, that is, the matching procedure is performed in a square that is 3 times larger than the max of width and height of bounding box of the hole. Then, for the structure offsets O_s, we calculate their statistics by a 2-d histogram $h_s(u, v)$ as

$$h_s(u, v) = \sum_x \delta(O(x) = (u, v)) \qquad (7)$$

where $\delta(\cdot)$ is 1 when the argument is true and 0 otherwise. The top k_1 peaks from the histogram are chosen as the k_1 dominant desired structure offsets. For non-structure part I_{ns}, k_2 dominant desired non-structure offsets are selected in the same way as for I_s. Therefore, there are $k = k_1 + k_2$ candidate offsets are selected. In our final implementation, $N = 8, k_1 = 40, k_2 = 20$ is the default configuration, and we also investigate their influence on the final inpainting performance in Section IV-A.

B. ENERGY EQUATION CONSTRUCTION

Instead of only using color information, multi-direction features based on Curvelet transform are exploited to construct energy equation in order to better maintain neighborhood consistence. The overall procedure of our energy equation construction is sketched in Figure 4. The data term E_d remains unchanged, that is, E_d is 0 if the label o_i is valid for x, otherwise E_d is $+\infty$. The smooth term E_s aims to penalize incoherent seams. For example, let o_a and o_b are two labels respectively assigned to x and x'. If $o_a \neq o_b$, then a seam will be appeared between x and x'. In order to avoid incoherent seam as much as possible, the multi-direction features are introduced into E_s. Denoting $a = L(x)$ and $b = L(x')$, our smooth term is defined as

$$\begin{aligned} E_s(a, b) = (&\|I(x + o_a) - I(x + o_b)\|^2 \\ &+ \|I(x' + o_a) - I(x' + o_b)\|^2) \\ &+ \lambda(\|F(x + o_a) - F(x + o_b)\|^2 \\ &+ \|F(x' + o_a) - F(x' + o_b)\|^2) \end{aligned} \qquad (8)$$

In the equation, $I(x)$ and $F(x)$ are respectively the RGB color values and N direction feature intensities of x, and λ is a coefficient balancing the color and multi-direction feature.
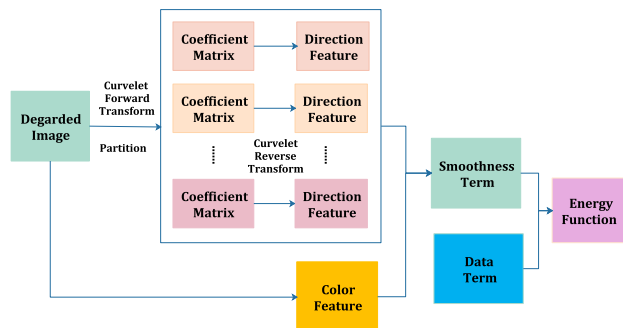
FIGURE 4. The frame diagram of energy equation construction.

Here, the multi-direction feature term $F(x)$ is referred by Curvelet transform, that is, after performing Curvelet forward transform and partitioning coefficient matrix set Q, the multi-direction matrix $F = \{F_n, n = 1, \cdots, N\}$ is obtained by

$$F_n = T^-(Z_n) \tag{9}$$

where T^- denotes Curvelet inverse transform. Equation (9) is slightly different from (5) in that only high frequency coefficients are applied to infer different direction features. To better maintain neighborhood consistence, all N direction features are applied to construct smooth term. Then combining the data term, the energy equation is constructed, which is later solved by multi-label graph-cuts algorithm [37].

C. ALGORITHM ANALYSIS
By integrating our labels selection and energy equation construction into the framework of MRF-based algorithms, the proposed SOS algorithm is developed. The pesu-docode of SOS is given in Algorithm 1. In the experiment, we implement two SOS versions with direction number $N = 4$ and $N = 8$. This work inherits our previous work [36]. Although both work utilize direction features as extra information to guide inpainting procedure, the degrees of exploitation of direction features are significantly different. For the labels selection scheme, on the one hand, the coefficient matrix Q undertakes a preprocess as (4), which is beneficial to more accurately extract direction features for further processing. On the other hand, the variance of local direction gradient magnitude was calculated to determine which direction feature image is used for matching similar patches in [36]. While in this work we combine all N direction features together for matching similar patches to obtain robust guiding information, which is much of benefit especially when the information around the damaged area is quite mess. Therefore, structure coherence can be better maintained. For the energy equation construction scheme, only color information was considered in [20], [26], [36], while in this work multi-direction features are further exploited to construct a smooth term that is able to better maintain neighborhood consistence for the inpainted images. In addition, we consider different numbers of direction in the current work, i.e., $N = 4$ and $N = 8$, while only four directions was considered in the previous work.

Algorithm 1 Pseudocode of SOS

Require: the degraded image I, the parameters α, k_1, k_2, λ
Ensure: the inpainted image
1: Transform I into YUV space and obtain the Y component as I_Y
2: Obtain coefficient matrix $\{Q_{s,d}\}$ on I_Y according to (3)
3: Perform preprocess on $\{Q_{s,d}\}$ according to (4)
4: Partition $\{Q'_{s,d}\}$ into N sets, resulting $Z_1, \cdots, Z_N$
5: Generate direction images A_n according to (5), $n = 1, \cdots, N$
6: Generate edge images B_n by performing canny operator and morphological operation on A_n, $n = 1, \cdots, N$
7: Stack edge images $B_1, B_2, \cdots, B_N$ into a whole edge image B
8: Partition I into structure part I_s and non-structure part I_{ns} via $I_s = I \cdot B$ and $I_{ns} = I \backslash I_s$
9: Obtain offsets for I_s and I_{ns} according to (6)
10: Calculate 2-d histograms $h_s(u, v)$ and $h_{ns}(u, v)$ according to (7)
11: Choose top k_1 and k_2 peaks from $h_s(u, v)$ and $h_{ns}(u, v)$ as candidate labels
12: Generate multi-direction matrix F according to (9)
13: Construct smooth term E_s according to (8)
14: Construct energy equation E according to (1) using the above E_s
15: Obtain labels by solving E using multi-label graph-cuts algorithm
16: Fill missing pixels/patchs using the labels

The computational complexity of the proposed SOS method is reasonable. Compared to most MRF-based algorithms, the main complexity difference is determined by the number of offsets for solving energy function. The computational cost is huge when all possible labels are applied, like the Shift-map approach in [20]. To the contrary, we elaboratively select only a few candidate offsets from structure and non-structure parts, which sharply reduces computation time. Compared with our previous work [36], only an extra Curvelet inverse transform operation is added for constructing smooth term, however, it hardly increases computational overhead because a fewer iterations may required to find the minimum value. In the next section, we will experimentally validate the effectiveness and efficiency of our method by inpainting different types of images.

IV. EXPERIMENTAL RESULTS
In this section, a mount of experiments are conducted to validate the superiority of our proposed approach. Firstly, the parameter setting is empirically discussed in order to give a default configuration. Then, the performance of our method is evaluated on inpainting various kinds of images and compared with several state-of-the-art methods. Finally, the effectiveness of proposed labels selection and energy function construction schemes are validated. All the experiments are
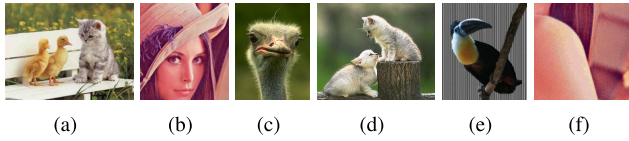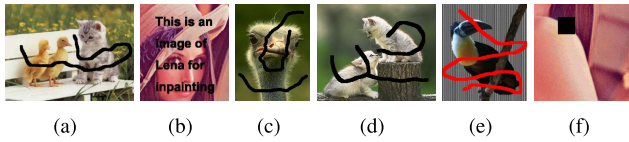
FIGURE 5. Original images.

FIGURE 6. Degraded images.

carried out on the platform of a PC with 4.0 GHz CPU, 16GB RAM and Matlab.

A. PARAMETER DISCUSSION

There are a few relatively important parameters need to be set in the proposed method, including threshold α in (4), weight λ in (8), and the numbers k_1 and k_2 of candidate offsets for structure and non-structure parts. To evaluate their influence and provide a proper setting, we test our algorithm with different settings in six images, as presented in Figures 5 and 6. To ensure a brief and efficient discussion, N is set to 8, the total number $k = k_1 + k_2$ of candidate labels is set to 60, and a setting with $\alpha = 0.8$, $\lambda = 0.5$, $k_1 = 40$ (therefore $k_2 = 20$) is applied as a default setting according to a pre-experiment. In this experiment, we only vary one parameter and keep others unchanged. The PSNR (in dB) is adopted to quantify inpainting performance.

We vary the threshold α in the range of [0, 1] with an interval 0.1, the weight λ in the range of [0, 2] with an interval 0.25, and the parameter k_1 in the range of [0, 60] with an interval 5. The PSNR values of each algorithm setting on inpainting six images in Figure 6 are plotted in Figures (7)-(9). Figure 7(a) shows that the inpainted images achieve relatively large PSNR values when α is set to 0.8, and it is also verified by Figure 7(b). Similarly, Figure 8 shows that a value of 0.5 for λ produces the best results among all the settings. Figure (9) reflects that the number of structure candidate labels indeed influent the inpainting performance. Specifically, the PSNR value increases to a peak when k_1 increases to 40, and then decreases as the value of k_1 keeps increasing. The reason is that structure candidate labels can provide plentiful structure priori for guiding inpainting process, however, a too large k_1 value will cover up the non-structure prior which may also required for inpainting tasks. According to the discussion, the default setting is applied to conduct further experiments.

B. PERFORMANCE COMPARISONS

In this section, we evaluate our algorithm performance on five kinds of inpainting tasks, including scratch and text removal, inpainting texture images, inpainting images with single direction structures, multi-direction structures and curve structures. Also, we compare the performance against four state-of-the-art exemplar-based algorithms,

including a greedy-based method (Wang *et al.* [17]), and three MRF-based methods (Le Meur *et al.* [38], He and Sun [26], and our recently work Cheng and Li [36]). Wang's method [17] is a greedy-based method that modified Criminisi's [39] priority function and used fast flourier transform to find more suitable candidate patch. In Le Meur *et al.* [38], several inpainting procedures with different parameter settings are first executed on a low-resolution image and then the results are fused together to produce a unique low-resolution image. Afterwards, a single image super-resolution algorithm is applied to obtain final result. He and Sun [26] computed offsets statistics in known region and chose some dominant offsets to be labels. Our previous work and Li [36] applied a direction structure distribution analysis scheme to choose a few dominant offsets, while keeping the energy equation the same as He and Sun [26]. In the experiments, all four compared algorithms utilize the settings as in their original papers. It needs to be pointed out that, because our recent work [36] has shown its superiority over eight other methods (including three greedy-based and five MRF-based methods) and this work is a further investigation, we only apply four algorithms (including our previous method [36]) as the compared ones in this experiment.

#### 1) COMPARISON ON SCRATCH AND TEXT REMOVAL

Five images with moderate composite structures but different backgrounds are used for scratch and text removal performance comparison, given in Figure 10. The inpainted results of Wang's, Le Meur's, He's, Cheng's and the proposed method are given in the third to seventh columns, respectively. The red rectangular block in some images highlights the part of an image suffering structure inconsistence or noticeable artifacts. For Wang's approach, structure incoherence appears in all results except Figure 10(d), especially some unwanted structures exist as illustrated in Figures 10(c) and 10(e). Le Meur's method could not achieve pleasant results in all tests due to the structure incoherence as shown in the fourth column of Figure 10. Moreover, relatively obvious inpainting marks and unwanted structures exist in Figures 10(b) and 10(d). The results of He's method have similar flaws on all images except the fourth one. Cheng's results seem to be better than these three algorithms, but structure incoherence still exists, as shown in Figures 10(c) and 10(e). The last column reflects that our proposed method obtains more pleasant inpainted results than the others, and the structure coherence and neighborhood consistence are maintained very well, though there are quit a few invisible mark in Figure 10(e). Tables 1 and 2 list PSNR and SSIM [40] values of the inpainted results obtained by five methods. According to the tables, the proposed method achieves the largest PSNR and SSIM values among all algorithms on each image, which validates the superior of our method on scratch and text removal. In addition, according to the computation time in Table 3, our method is more efficient than Wang's and Le Meur's methods in a large degree, and has almost the same efficient as He's and Cheng's methods.
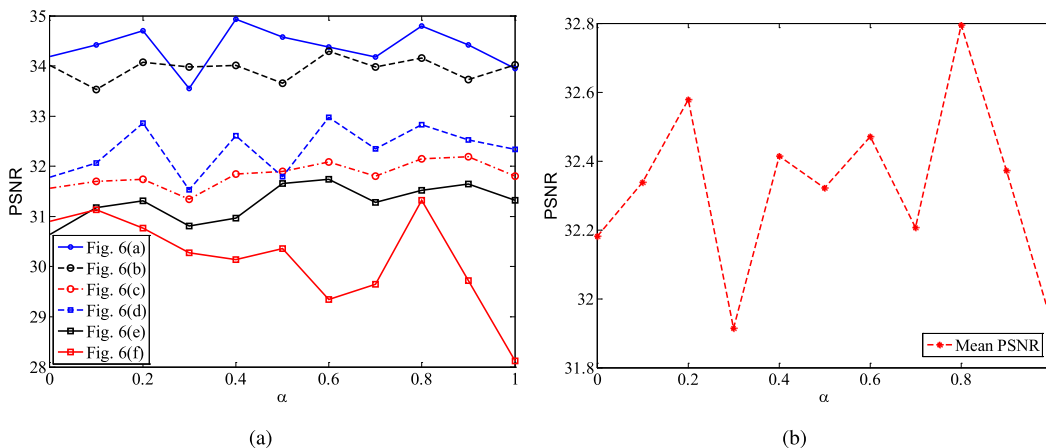
FIGURE 7. PSNR curves varied with different α values. Figure 7(a) is the PSNR curves for inpainting each image in Figure 6, and Figure 7(b) gives the mean PSNR curve.
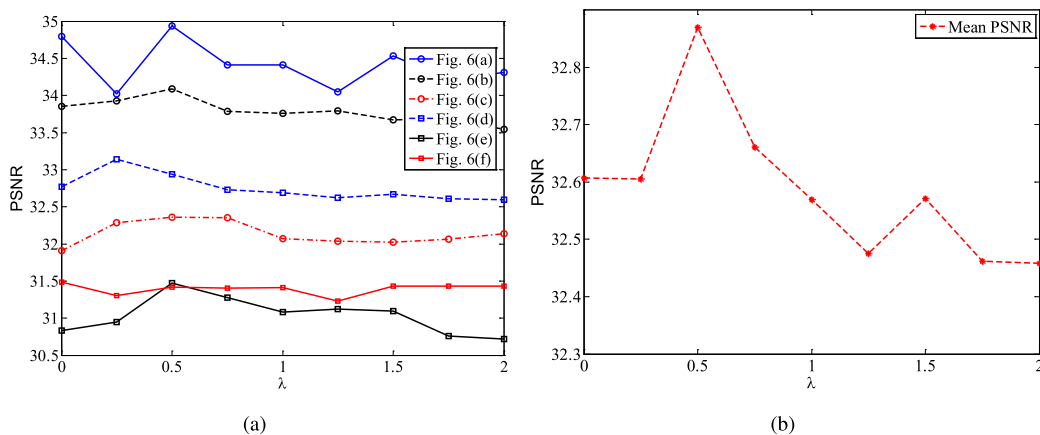
FIGURE 8. PSNR curves varied with different λ values. Figure 8(a) is the PSNR curves for inpainting each image in Figure 6, and Figure 8(b) gives the mean PSNR curve.
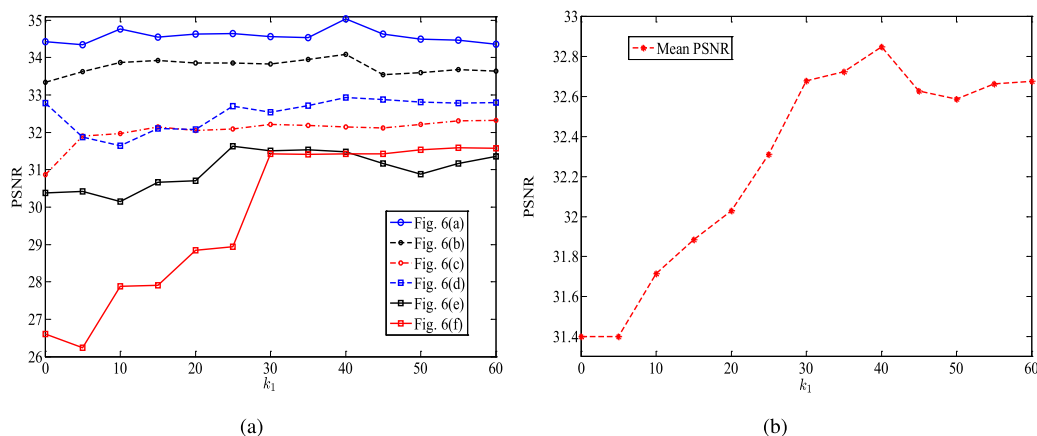
FIGURE 9. PSNR curves varied with different k_1 values. Figure 9(a) is the PSNR curves for inpainting each image in Figure 6, and Figure 9(b) gives the mean PSNR curve.

2) COMPARISON ON INPAINTING TEXTURE IMAGES

Figure 11 gives the results of five algorithms on inpainting texture images without obvious structures. We can find that error accumulation phenomenon appears in Wang's results,

illustrated in Figures 11(a) and 11(c). The MRF-based methods can produce better results than Wang's greedy-based method, however, some artificial effects exist in Le Meur's results, as shown in Figures 11(a) and 11(c). As for He's,

(a)

(b)

(c)

(d)

(e)
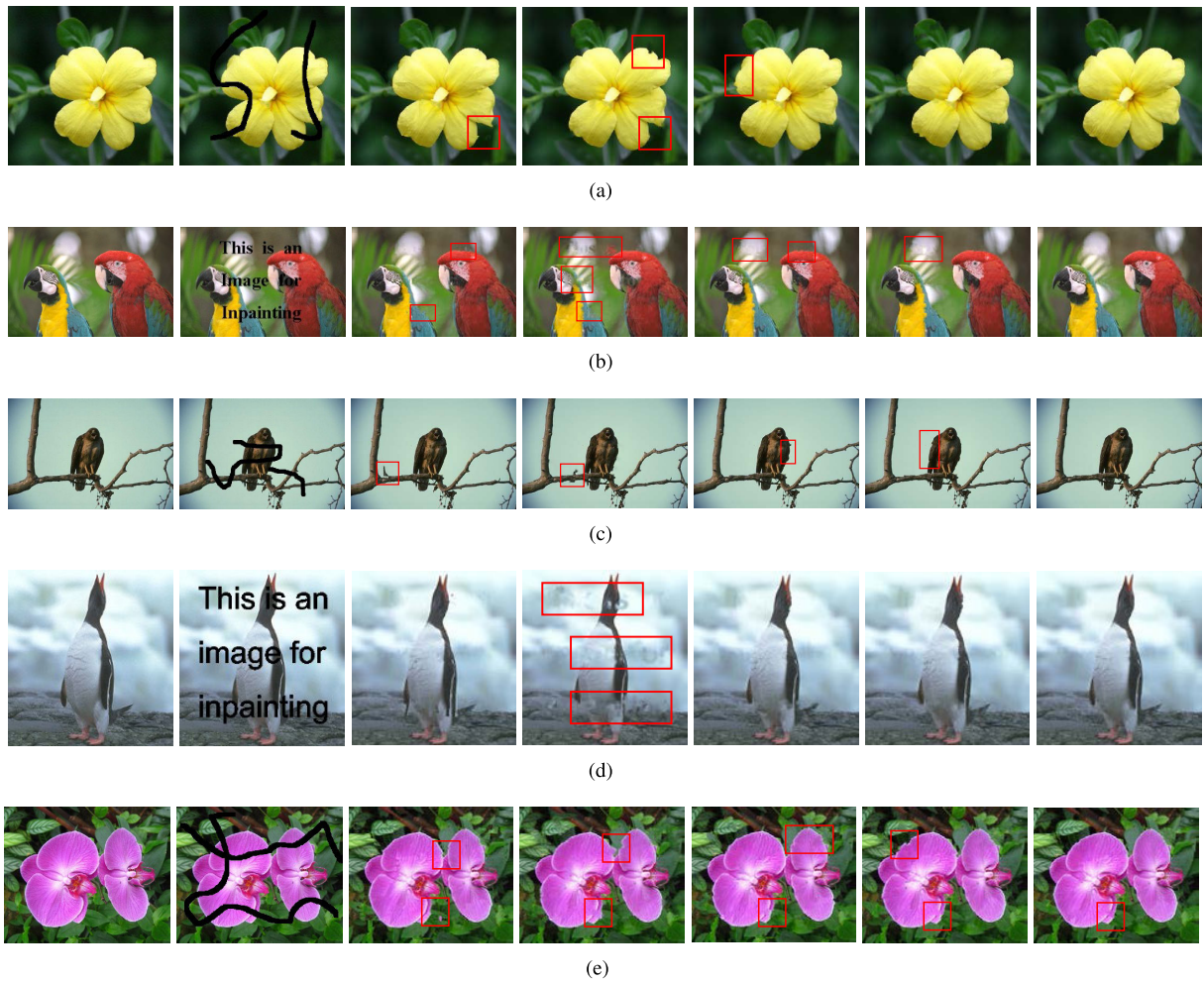
FIGURE 10. Performance comparisons on scratch and test removal. For each row, the columns from left to right are the original image, degraded image, inpainted results of Wang's, Le Meur's, He's, Cheng's and the proposed methods, respectively.

TABLE 1. PSNR (in dB) comparisons on scratch and text removal.

	Wang [17]	Le [38]	He [26]	Cheng [36]	SOS
Figure 10(a)	35.26	32.75	35.29	35.76	38.56
Figure 10(b)	31.92	29.17	31.36	31.77	35.65
Figure 10(c)	31.65	30.11	31.49	32.72	35.54
Figure 10(d)	32.29	29.24	32.62	32.93	37.54
Figure 10(e)	27.49	26.52	26.81	27.48	30.47
Mean value	31.72	29.56	31.51	32.03	**35.55**

TABLE 2. SSIM comparisons on scratch and text removal.

	Wang [17]	Le [38]	He [26]	Cheng [36]	SOS
Figure 10(a)	0.9738	0.9735	0.9732	0.9734	0.9812
Figure 10(b)	0.9700	0.9474	0.9662	0.9637	0.9842
Figure 10(c)	0.9811	0.9753	0.9829	0.9822	0.9865
Figure 10(d)	0.9509	0.9177	0.9455	0.9492	0.9717
Figure 10(e)	0.9010	0.8881	0.8939	0.8902	0.9232
Mean value	0.9554	0.9404	0.9523	0.9517	**0.9693**

TABLE 3. Computation time (in seconds) comparisons on scratch and text removal.

	Wang [17]	Le [38]	He [26]	Cheng [36]	SOS
Figure 10(a)	1047.4	157.2	12.7	11.6	11.2
Figure 10(b)	780.8	137.8	9.4	9.2	5.0
Figure 10(c)	2491.4	226.7	10.6	18.9	17.6
Figure 10(d)	1111.8	218.3	10.0	6.3	9.1
Figure 10(e)	959.3	195.2	11.2	11.49	10.7
Mean value	1278.1	187.0	10.8	11.5	**10.7**

TABLE 4. Computation time (in seconds) comparisons on inpainting textural images.

	Wang [17]	Le [38]	He [26]	Cheng [36]	SOS
Figure 11(a)	3988.5	199.8	15.8	10.6	10.6
Figure 11(b)	5749.2	141.8	19.7	14.1	22.5
Figure 11(c)	476.8	194.5	3.0	2.6	3.1
Mean value	3404.8	178.7	12.8	**9.1**	12.1

Cheng's and ours results, they all look natural and coherent. According to the computation time listed in Table 4, we can say that the computation complexity of our method is far less than Wang's and Le Meur's methods and almost the same as He's and Cheng's methods. In summary, our proposed method can achieve pleasant inpainted results with a high efficient.

(a)

(b)

(c)
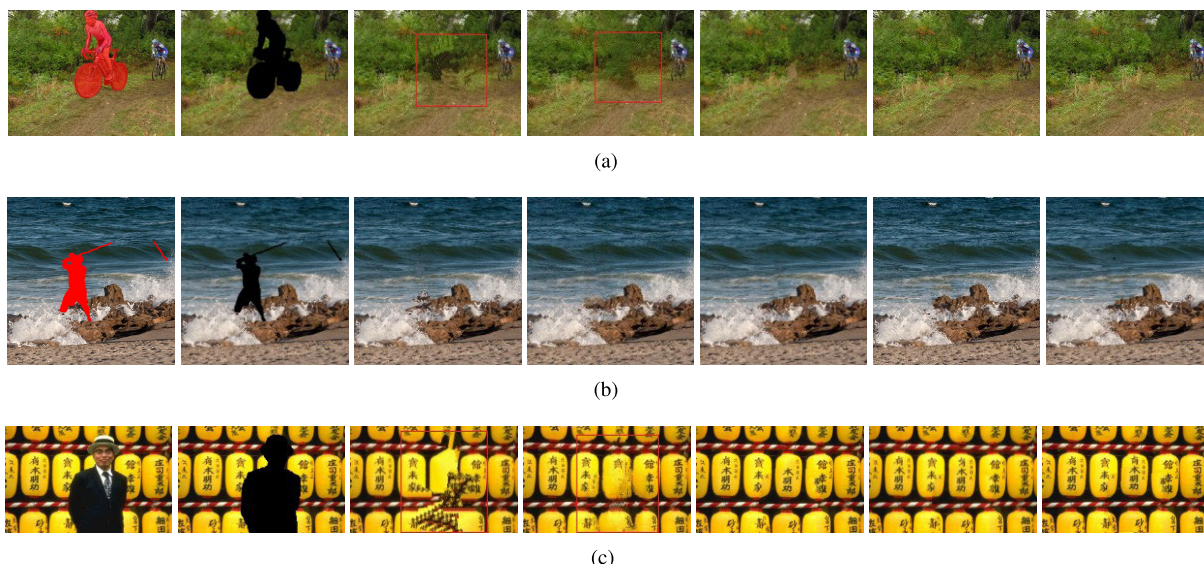
FIGURE 11. Performance comparisons on inpainting texture images. For each row, the columns from left to right are the original image, degraded image, inpainted results of Wang's, Le Meur's, He's, Cheng's and the proposed methods, respectively.

(a)

(b)

(c)

(d)
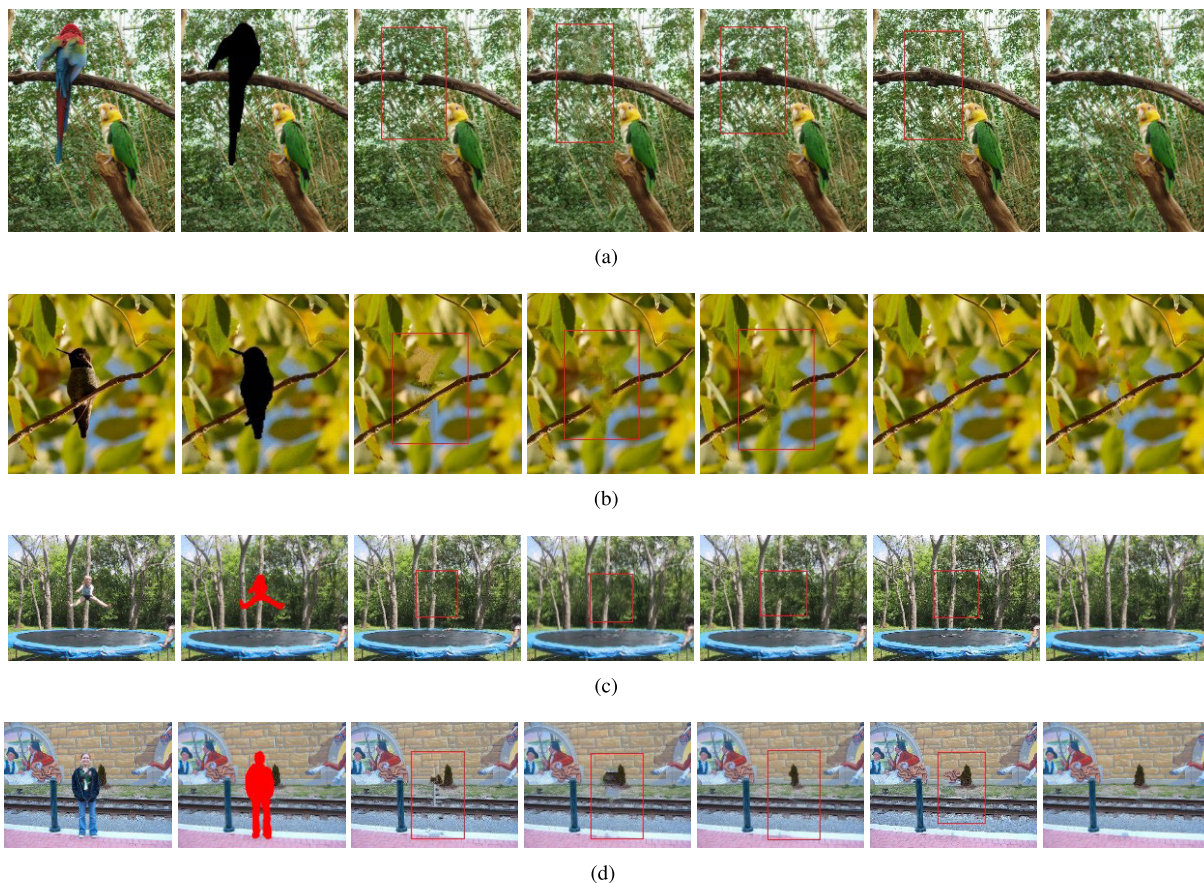
FIGURE 12. Performance comparisons on inpainting with single direction structures. For each row, the columns from left to right are the original image, degraded image, inpainted results of Wang's, Le Meur's, He's, Cheng's and the proposed methods, respectively.

3) COMPARISON ON INPAINTING IMAGES WITH SINGLE DIRECTION STRUCTURE

The main purpose of our method is to maintain structure coherence and neighborhood consistence of inpainted results, therefore we test our algorithm performance on inpainting images with various kinds of structures. In this experiment, four images with single direction structures and different backgrounds are inpainted, and the results of five algorithms are illustrated in Figure 12. According to the Figures, we can see that Wang's results are not satisfied since not only the
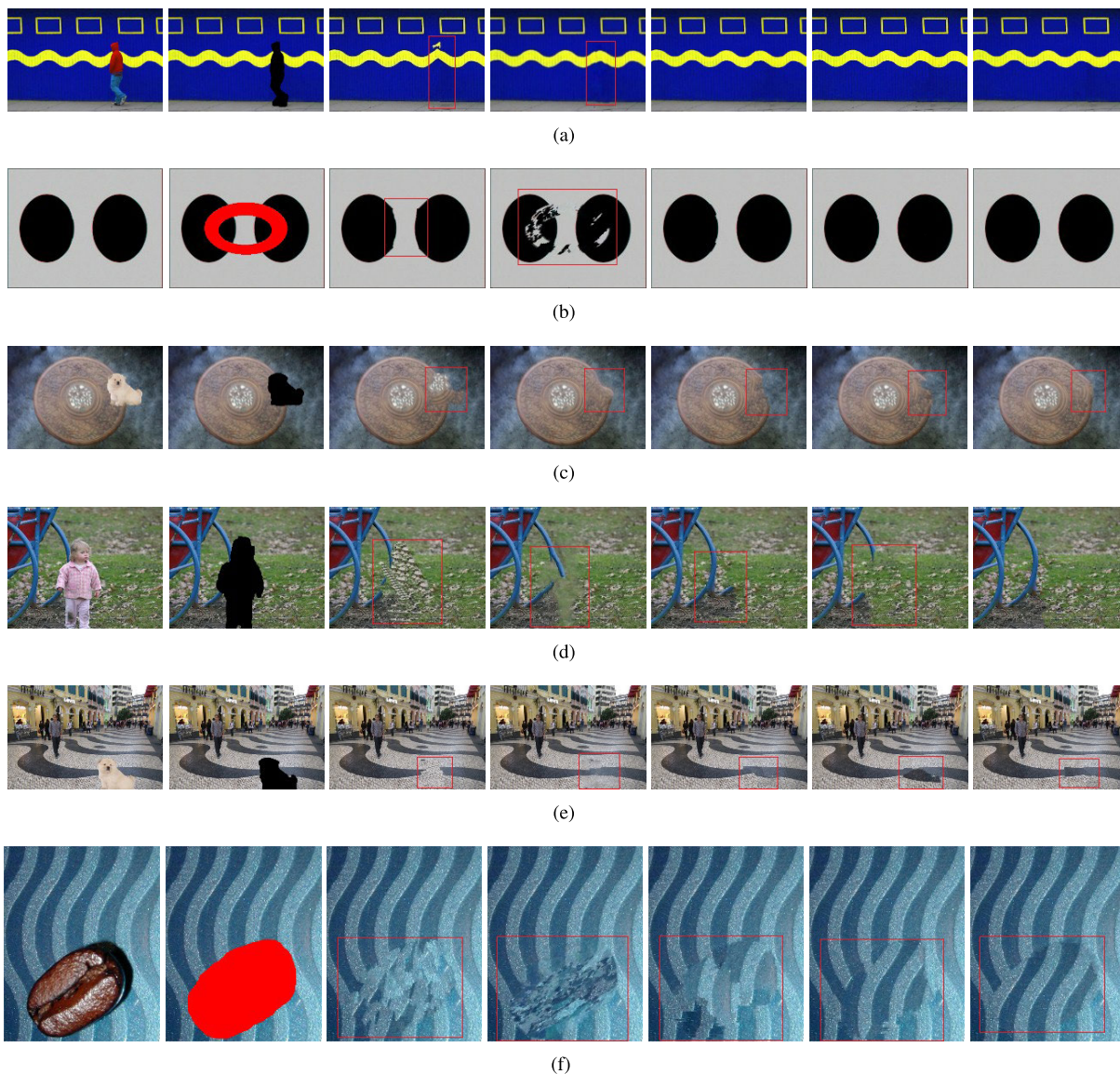
(a)

(b)

(c)

(d)

(e)

FIGURE 13. Performance comparisons on inpainting with multi-direction structures. For each row, the columns from left to right are the original image, degraded image, inpainted results of Wang's, Le Meur's, He's, Cheng's and the proposed methods, respectively.

structures are incoherent but also seam effects and error accumulation phenomenon exist. The cause is as a greedy-based method it utilizes a greedy filling procedure and the error accumulation phenomenon is inevitable. For MRF-based methods, the structure coherence is not always well maintained by Le Meur's method, as shown in Figures 12(b) and 12(c), and some inpainted trails appear in all results. He's approach fails to repair images with relative less structures, as shown in Figures 12(b) and 12(c). Cheng's method obtains relatively better inpainted results. However, it fails to repair images with complex structures like Figures 12(c) and 12(d). To the contrary, our method is able to well maintain structure coherence and neighborhood consistence in all images and the inpainted images look natural.

4) COMPARISON ON INPAINTING IMAGES WITH MULTI-DIRECTION STRUCTURE

To verify the performance on images with multi-direction structures, five images are inpainted and the results are presented in Figure 13. From the results, we can see that

structure incoherence appears in Wang's results, particularly error accumulation phenomenon is serious. Viewing Le Meur's results, structure incoherence also appears, and some unwanted context exists as shown in Figure 13(d). Though He'e method applies offsets statistics to guide filling procedure, it still cannot maintain structure coherence well according to Figures 13(a), 13(b) and 13(d). The reason is when the original structure information is diverse and not sufficient, the desired structure labels would be swept under other labels during candidate labels selection procedure. As the desired direction features are selected, Cheng's results are better than He's, however, it still fails to recover images with relatively less and complex structures like Figures 13(a) and 13(b). Because our method extracts plentiful multi-direction edge information to distinguish structure and non-structure labels and applies multi-direction features to construct smooth term, more pleasant results are obtained as shown in Figures 13. Although the structure coherence is not quite well maintained in Figure 13(e), the repaired result still looks natural and coherent, and satisfies human eye visual requirements.

FIGURE 14. Performance comparisons on inpainting with curve direction structures. For each row, the columns from left to right are the original image, degraded image, inpainted results of Wang's, Le Meur's, He's, Cheng's and the proposed methods, respectively.

5) COMPARISON ON INPAINTING IMAGES WITH CURVE STRUCTURE

To show the superiority of our method on maintaining structure coherence, six images with more complex structures, i.e., curve structures, are inpainted, and the results are given in Figure 14. According to Figures 14(a) and 14(b), we can see that He's, Cheng's and our methods can repair images with repetitive curve structure very well, while the other two works badly. On inpainting image with complex curve structure and simple background, our method are much better than other four ones, as shown in Figure 14(c). For image with curve structure and complex texture background in Figure 14(d), our method can maintain structure coherence and neighborhood consistence at the same time. As for Figure 14(e), there is complex missing curve structure while no exactly the same curve structure exists

in known region, our method still obtains relatively better repaired result. For Figure 14(f), since the known region contains only a few curve structure similar to the missing content, our method could not obtain a inpainted result satisfied with human eye visual requirements very well. However, Our method extends the structure along the direction of the structures in known region and the inpainted result is more naturally than other four results. The reason of such good performance comes from the reasonable labels and the smooth term in energy equation where multi-direction features are elaborately exploited with the aim of maintaining structure coherence and neighborhood consistence.

C. VALIDATION OF THE COMPONENTS
The previous experiments verify the superiorities of our proposed method over several compared algorithms on

TABLE 5. PSNR (in dB) comparisons of six SOS variants and Cheng's method [36] on inpainting images in Figure 6.

	Cheng [36]	SOS4-*L*	SOS4-*E*	SOS4-*LE*	SOS8-*L*	SOS8-*E*	SOS8-*LE*
Figure 6(a)	33.69	34.49	34.24	34.85	34.51	34.22	34.82
Figure 6(b)	28.05	28.86	28.25	29.65	30.59	28.29	31.57
Figure 6(c)	31.43	32.31	31.99	32.20	32.62	32.17	33.13
Figure 6(d)	31.85	32.13	32.21	32.57	32.29	32.33	32.54
Figure 6(e)	33.71	34.07	33.77	34.34	34.06	33.92	34.28
Figure 6(f)	31.07	31.67	31.59	31.82	31.75	31.54	31.89
Mean value	31.63	32.26	32.01	32.57	32.64	32.08	**33.04**

inpainting five kinds of images. In order to further validate the effectiveness of proposed labels selection and energy equation schemes by exploiting image multi-direction features, we test six variants of our proposed SOS method on inpainting the images in Figure 6. We denote six variants in a form of SOSN-X. N is the number of direction partitions and $N \in \{4, 8\}$ is tested. $X \in \{L, E, LE\}$ denotes the components used in the variants, where L means the proposed label selection scheme is applied and the energy equation is the same as in our previous work [36], E means the proposed energy equation is applied while label selection scheme is the same as in [36], and LE denotes two proposed schemes are applied (Hence, $SOS8$-LE is the algorithm verified in the previous experiments). Since the current work is a further continuation and deepening of our previous work [36], it is applied a baseline to verify the superiority of current work. The PSNR comparisons of six SOS variants as well as Cheng's method are listed in Table 5. According to the results, three conclusions can be made. First, the proposed labels selection and energy equation schemes indeed enhance the inpainting performance. Second, the two schemes can cooperatively improve the performance in a large degree. Third, the number of direction partition truly influent the algorithm performance. But taking effectiveness and efficiency into account, we recommend using $N = 8$ as a default setting.

V. CONCLUSION

In this paper, we introduced a novel MRF-based inpainting method that exploits image multi-direction features to guide inpainting procedures with the purpose of maintaining structure coherence and neighborhood consistence of inpainted images. To effectively and efficiently select proper labels for MRF nodes, the image is partitioned into structure and non-structure images, where the structure part is stacked with several edge images on different direction features. The offsets are matched independently in two parts and a few dominant ones are selected as labels. When constructing energy equation, multi-direction features are used to devise a smooth term. We have demonstrated the superiority of our method over some state-of-the-art approaches on inpainting various kinds of degraded images. In addition, the effectiveness of two new ingredients as well as the experiment settings are empirically investigated. Our method is based on an in-depth exploitation of image direction features. We believe it would

be an effect way to solve more difficult inpainting tasks like the images with complex curved structures via exploiting some other curve features, and we will further investigate this in our future work.

REFERENCES

[1] M. Bertalmio, G. Sapiro, V. Caselles, and C. Ballester, "Image inpainting," in *Proc. Int. Conf. Comput. Graph. Interact. Techn.*, 2000, pp. 417–424.

[2] C. Guillemot and O. Le Meur, "Image inpainting : Overview and recent advances," *IEEE Signal Process. Mag.*, vol. 31, no. 1, pp. 127–144, Jan. 2014.

[3] M. Bertalmio, A. L. Bertozzi, and G. Sapiro, "Navier-stokes, fluid dynamics, and image and video inpainting," in *Proc. IEEE Comput. Soc. Conf. Comput. Vis. Pattern Recognit.*, Dec. 2001, pp. 355–362.

[4] J. Shen and T. F. Chan, "Mathematical models for local nontexture inpainting," *SIAM J. Appl. Math.*, vol. 62, no. 3, pp. 1019–1043, 2002.

[5] T. F. Chan and J. Shen, "Nontexture inpainting by curvature-driven diffusions," *J. Vis. Commun. Image Represent.*, vol. 12, no. 4, pp. 436–449, 2001.

[6] M. Elad, J.-L. Starck, P. Querre, and D. L. Donoho, "Simultaneous cartoon and texture image inpainting using morphological component analysis (MCA)," *Appl. Comput. Harmon. Anal.*, vol. 19, no. 3, pp. 340–358, 2005.

[7] K.-M. Hung, Y.-L. Chen, and C.-T. Hsieh, "A novel bandelet-based image inpainting," *IEICE Trans. Fundam. Electron., Commun. Comput. Sci.*, vol. 92, no. 10, pp. 2471–2478, 2009.

[8] J. Mairal, M. Elad, and G. Sapiro, "Sparse representation for color image restoration," *IEEE Trans. Image Process.*, vol. 17, no. 1, pp. 53–69, Jan. 2008.

[9] M. J. Fadili, J.-L. Starck, and F. Murtagh, "Inpainting and zooming using sparse representations," *Comput. J.*, vol. 52, no. 1, pp. 64–79, Jan. 2009.

[10] J. Mairal, F. Bach, J. Ponce, and G. Sapiro, "Online learning for matrix factorization and sparse coding," *J. Mach. Learn. Res.*, vol. 11, pp. 19–60, Mar. 2010.

[11] R. Ma, N. Barzigar, A. Roozgard, and S. Cheng, "Decomposition approach for low-rank matrix completion and its applications," *IEEE Trans. Signal Process.*, vol. 62, no. 7, pp. 1671–1683, Apr. 2014.

[12] F. Wen, L. Adhikari, L. Pei, R. F. Marcia, P. Liu, and R. C. Qiu, "Nonconvex regularization-based sparse recovery and demixing with application to color image inpainting," *IEEE Access*, vol. 5, pp. 11513–11527, 2017.

[13] A. Wong and J. Orchard, "A nonlocal-means approach to exemplar-based inpainting," in *Proc. 15th IEEE Int. Conf. Image Process.*, Oct. 2008, pp. 2600–2603.

[14] Z. Xu and J. Sun, "Image inpainting by patch propagation using patch sparsity," *IEEE Trans. Image Process.*, vol. 19, no. 5, pp. 1153–1165, May 2010.

[15] J. Wang, K. Lu, D. Pan, N. He, and B.-K. Bao, "Robust object removal with an exemplar-based image inpainting approach," *Neurocomputing*, vol. 123, pp. 150–155, Jan. 2014.

[16] Z. Li, H. He, H. M. Tai, Z. Yin, and F. Chen, "Color-direction patch-sparsity-based image inpainting using multidirection features," *IEEE Trans. Image Process.*, vol. 24, no. 3, pp. 1138–1152, Mar. 2015.

[17] H. Wang, L. Jiang, R. Liang, and X.-X. Li, "Exemplar-based image inpainting using structure consistent patch matching," *Neurocomputing*, vol. 269, pp. 90–96, Dec. 2017.

[18] H. Liu, X. Bi, G. Lu, W. Wang, J. Yan, and Z. Zhang, "Screen window propagating for image inpainting," *IEEE Access*, vol. 6, pp. 61761–61772, 2018.

[19] N. Komodakis and G. Tziritas, "Image completion using efficient belief propagation via priority scheduling and dynamic pruning," *IEEE Trans. Image Process.*, vol. 16, no. 11, pp. 2649–2661, Nov. 2007.

[20] Y. Pritch, E. Kav-Venaki, and S. Peleg, "Shift-map image editing," in *Proc. IEEE 12th Int. Conf. Comput. Vis.*, Sep./Oct. 2009, pp. 151–158.

[21] J. Xie, L. Xu, and E. Chen, "Image denoising and inpainting with deep neural networks," in *Proc. Adv. Neural Inf. Process. Syst.*, 2012, pp. 341–349.

[22] R. Köhler, C. Schuler, B. Schölkopf, and S. Harmeling, "Mask-specific inpainting with deep neural networks," in *Proc. German Conf. Pattern Recognit.*, 2014, pp. 523–534.

[23] V. K. Alilou and F. Yaghmaee, "Application of GRNN neural network in non-texture image inpainting and restoration," *Pattern Recognit. Lett.*, vol. 62, pp. 24–31, Sep. 2015.

[24] N. Cai, Z. Su, Z. Lin, H. Wang, Z. Yang, and B. W. Ling, "Blind inpainting using the fully convolutional neural network," *Vis. Comput.*, vol. 33, no. 2, pp. 249–261, 2017.

[25] G. Liu, F. A. Reda, K. J. Shih, T.-C. Wang, A. Tao, and B. Catanzaro, "Image inpainting for irregular holes using partial convolutions," in *Proc. Eur. Conf. Comput. Vis. (ECCV)*, 2018, pp. 89–105.

[26] K. He and J. Sun, "Image completion approaches using the statistics of similar patches," *IEEE Trans. Pattern Anal. Mach. Intell.*, vol. 36, no. 12, pp. 2423–2435, Dec. 2014.

[27] W. Xue and R. Zhang, "Graph-based image completion using patch offsets and structure feature," in *Proc. Int. Conf. Graph. Image Process.*, 2014, p. 9069.

[28] Y. Liu and V. Caselles, "Exemplar-based image inpainting using multiscale graph cuts," *IEEE Trans. Image Process.*, vol. 22, no. 5, pp. 1699–1711, May 2013.

[29] T. Ružić and A. Pižurica, "Context-aware patch-based image inpainting using Markov random field modeling," *IEEE Trans. Image Process.*, vol. 24, no. 1, pp. 444–456, Jan. 2015.

[30] S. Ge, K. Xie, S. Li, and R. Yang, "Global image completion with joint sparse patch selection and optimal seam synthesis," *Signal Process.*, vol. 124, pp. 147–155, Jul. 2016.

[31] D. Gupta, V. Chhajer, A. Mishra, and C. V. Jawahar, "A non-local MRF model for heritage architectural image completion," in *Proc. Conf. Comput. Vis., Graph. Image Process.*, 2012, pp. 61–68.

[32] A. Bugeau, M. Bertalmío, V. Caselles, and G. Sapiro, "A comprehensive framework for image inpainting," *IEEE Trans. Image Process.*, vol. 19, no. 10, pp. 2634–2645, Oct. 2010.

[33] M. Ghorai, S. Mandal, and B. Chanda, "A group-based image inpainting using patch refinement in MRF framework," *IEEE Trans. Image Process.*, vol. 27, no. 2, pp. 556–567, Feb. 2018.

[34] S. Darabi, E. Shechtman, C. Barnes, D. B. Goldman, and P. Sen, "Image Melding: Combining inconsistent images using patch-based synthesis," *ACM Trans. Graph.*, vol. 31, no. 4, p. 82, 2012.

[35] D. Jin and X. Bai, "Patch-sparsity-based image inpainting through a facet deduced directional derivative," *IEEE Trans. Circuits Syst. Video Technol.*, vol. 29, no. 5, pp. 1310–1324, May 2019.

[36] J. Cheng and Z. Li, "Markov random field-based image inpainting with direction structure distribution analysis for maintaining structure coherence," *Signal Process.*, vol. 154, pp. 182–197, Jan. 2019.

[37] Y. Boykov, O. Veksler, and R. Zabih, "Fast approximate energy minimization via graph cuts," *IEEE Trans. Pattern Anal. Mach. Intell.*, vol. 23, no. 11, pp. 1222–1239, Nov. 2001.

[38] O. Le Meur, M. Ebdelli, and C. Guillemot, "Hierarchical super-resolution-based inpainting," *IEEE Trans. Image Process.*, vol. 22, no. 10, pp. 3779–3790, Oct. 2013.

[39] A. Criminisi, P. Pérez, and K. Toyama, "Region filling and object removal by exemplar-based image inpainting," *IEEE Trans. Image Process.*, vol. 13, no. 9, pp. 1200–1212, Sep. 2004.

[40] Z. Wang, A. C. Bovik, H. R. Sheikh, and E. P. Simoncelli, "Image quality assessment: From error visibility to structural similarity," *IEEE Trans. Image Process.*, vol. 13, no. 4, pp. 600–612, Apr. 2004.
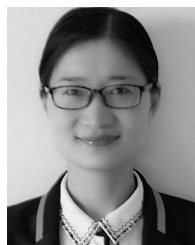
ZHIDAN LI received the B.S. degree in automation and the Ph.D. degree in signal and information processing from the School of Information Science and Technology, Southwest Jiaotong University, Chengdu, China, in 2008 and 2015, respectively. She is currently a Lecturer with Southwest Petroleum University, Chengdu, China. Her research interests include digital image inpainting and intelligent computing.
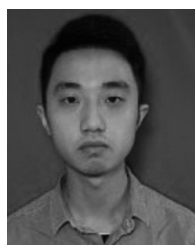
JIAWEI LIU received the B.S. degree in electrical engineering and its automation from Southwest Petroleum University, Chengdu, China, in 2018, where he is pursuing the M.S. degree in control engineering. His research interests include facial expression recognition and image recognition.
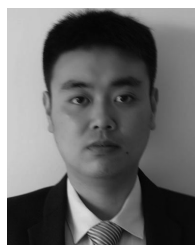
JIXIANG CHENG received the B.S. degree in automation, the M.S. degree in control engineering, and the Ph.D. degree in electrical engineering from Southwest Jiaotong University, Chengdu, China, in 2008, 2011, and 2015, respectively. He is currently an Associate Professor with Southwest Petroleum University, Chengdu. His current research interests include intelligent computing, image processing, and their applications.

• • •